Postprint of: Chlipała M., Błaszczak P., Wang S.-F., Jasiński P., Bochentyn B., In situ study of a composition of outlet gases from biogas fuelled Solid Oxide Fuel Cell performed by the Fourier Transform Infrared Spectroscopy, International Journal of Hydrogen Energy, Vol. 44, No. 26 (2019), pp. 13864-13874, DOI: 10.1016/j.ijhydene.2019.03.243

In situ study of a composition of outlet gases from biogas fuelled Solid Oxide Fuel Cell performed by the Fourier Transform Infrared Spectroscopy

M. Chlipała[a], P. Błaszczak[a], S.-F. Wang[b], P. Jasiński[c], B. Bochentyn[a,*]

[a]*Faculty of Applied Physics and Mathematics, Gdansk University of Technology, 80-233 Gdansk, ul. Narutowicza 11/12, Poland*
[b]*Faculty of Electronics, Telecommunications and Informatics, Gdansk University of Technology, 80-233 Gdansk, ul.Narutowicza 11/12, Poland*
[c]*Department of Material and Mineral Resources Engineering, National Taipei University of Technology, 1, Sec. 3, Zhongxiao E. Rd., Taipei, 106 Taiwan*

*corresponding author: beata.bochentyn@pg.edu.pl

Abstract

The purpose of this study was to develop a method and software based on the Fourier Transform Infrared Spectroscopy for the in-situ, quantitative analysis of the composition of outlet gases from Solid Oxide Fuel Cell (SOFC). The calibration procedure performed at the beginning of the experiment indicated a polynomial dependence between the concentration of a calibrating gas (CO, CO_2, CH_4) and the corresponding integrated absorbance in particular wavenumber ranges. Further, it allowed determining a concentration of CO_2, CO, CH_4 and H_2 in the outlet gas stream of the Ni–YSZ anode supported Direct Internal Reforming-SOFC fuelled by synthetic biogas (mixture of CO_2 and CH_4 in a volume ratio 2:3). The analysis was performed for over 90 h. Based on calculated concentration the conversion rates for both CH_4 and CO_2 gases were calculated, as well as the yields and selectivities of CO and H_2. Also, the carbon balance was determined. In order to predict the direction of particular reforming reactions, a non-equilibrium analysis was performed. Namely, a thermodynamic probability of solid carbon formation was obtained based on calculations of carbon activity coefficients. Obtained results indicated degradation of a fuel cell and corresponded well with electrical measurements where a decrease of power density in wet synthetic biogas was observed.

Keywords: *biogas reforming, direct internal reforming, carbon deposition, SOFC, FTIR, reaction quotient, carbon activity coefficient*

1. Introduction

Finite sources of fossil fuels and a continuously growing world's demand for energy have attracted considerable attention for alternative power sources. Thus, a significant research effort is devoted to the development of systems which utilize a wide variety of hydrocarbon fuels. Among them, Solid Oxide Fuel Cells (SOFCs) [1-8] and Molten Carbonate Fuel Cells (MCFCs) [9-11] can operate with alternative fuels, e.g. biogas. It is produced from anaerobic residual digestion of biomass [12,13] and is considered as a promising and environmental-friendly fuel because of its availability and renewability. Typically, it has a composition of approximately 50-80% CH_4 and 30-50% CO_2 with traces of H_2S, O_2, N_2 [13].

In the case of the biogas fed cells operating at high temperature (above 700 °C), the reforming process can be performed directly in the fuel cell leading to the production of H_2, CO and CO_2. In contrast, at low temperatures, the reforming should be performed before the gas reaches the fuel cell (external reforming). Since this process takes place outside the fuel cell, it requires an external heat source [11,14] extending costs of such a system. Currently, many groups are working on economically efficient direct internal reforming SOFC (DIR-SOFC) [15-21]. In that case, few reactions (Eg.1)-(Eq.10) occur in parallel within the anode volume. The main reforming reactions are steam reforming (Eq. 1) and dry reforming (Eq. 2). In steam reforming, the water, in a vapour state, is mixed with the methane to form hydrogen and carbon monoxide, while in dry reforming, the CO_2 reacts with the methane to form carbon monoxide and hydrogen [22-24].

$$CH_4 + H_2O \leftrightarrow CO + 3H_2 \qquad \Delta H = 206{,}2\,kJ/mol \qquad (1)$$

$$CH_4 + CO_2 \leftrightarrow 2CO + 2H_2 \qquad \Delta H = 247\,kJ/mol \qquad (2)$$

This hydrogen can be utilized in a direct reaction with carbon dioxide in a reverse water-gas shift reaction (Eq.3) or methanation process (Eq.4).

$$CO_2 + H_2 \leftrightarrow CO + H_2O \qquad \Delta H = 41\ kJ/mol \tag{3}$$

$$CO_2 + 4H_2 \leftrightarrow CH_4 + 2H_2O \qquad \Delta H = -165\ kJ/mol \tag{4}$$

The reverse water-gas shift (RWGS) reaction leads to the production of carbon monoxide and water, whereas within methanation water and methane are formed.

Moreover, the produced H_2, CO and supplied CH_4 can be electrochemically oxidized according to reactions described by Eqs. 5-7 [25, 26].

$$H_2 + O^{2-} \leftrightarrow H_2O + 2e^- \qquad \Delta H = -242\ kJ/mol \tag{5}$$

$$CO + O^{2-} \leftrightarrow CO_2 + 2e^- \qquad \Delta H = -283\ kJ/mol \tag{6}$$

$$CH_4 + O^{2-} \leftrightarrow 2H_2 + CO + 2e^- \qquad \Delta H = -37\ kJ/mol \tag{7}$$

However, direct SOFC feeding with hydrocarbons has some major drawbacks. When a traditional Ni– YSZ anode is applied, then a coking process occurs. As a result, both anode surface, pores and voids may be filled with carbon. It leads to bursting of the anode structure as well as to a decrease of an amount of catalytically active sites [24, 27-29]. The main causes of carbon deposition are pyrolysis (cracking) (Eq. 8), Boudouard reaction (Eq. 9) and carbon monoxide reduction (Eq. 10) [26].

$$CH_4 \leftrightarrow C + 2H_2 \qquad \Delta H = 74\ kJ/mol \tag{8}$$

$$2CO \leftrightarrow C + CO_2 \qquad \Delta H = -172\ kJ/mol \tag{9}$$

$$CO + H_2 \leftrightarrow C + H_2O \qquad \Delta H = -131\ kJ/mol \tag{10}$$

The pyrolysis is a decomposition process which occurs under the influence of high temperature and is carried out without the participation of oxygen. In the case of methane, it disintegrates into hydrogen and carbon. The Boudouard reaction is also a decomposition reaction. Metals, such as nickel catalyse it, and therefore there is a high risk of carbon deposition on the Ni-YSZ anode [24, 30]. The quantity of deposited carbon is strongly affected by the operating temperature and the methane/steam ratio. Removal of this carbon can be performed mainly via a reverse of reaction (Eq. 8) (with the usage of hydrogen additionally supplied or produced in reforming process) or via electrochemical oxidation of solid carbon (Eq. 11) [31]:

$$C + O^{2-} \leftrightarrow CO + 2e^- \qquad \Delta H = -110\ kJ/mol \tag{11}$$

In order to analyse a reforming process deeper, knowledge about the composition of outlet gases is required. The gas analysis methods include Gas Chromatography (GC), Secondary Ion Mass Spectrometry (SIMS) and Fourier Transform Infrared spectroscopy (FTIR).

Gas chromatography is an analytical technique based on the separation of complex mixtures. It was used i.a. by F. Santoni et al. [32] to study a gas composition on the anode site of operating SOFC. This approach proved to supply valuable information on the chemical and electrochemical reactions in SOFC utilizing CH_4 as a fuel. A uniformity of reforming reactions along the anode surface was also shown [33,34]. Although this technique is accurate for such analysis, it requires expensive equipment and can probe a relatively small flow rate compared to overall fuel flow. Moreover, GC measurement is based on a rate at which molecules progress in a column. This leads to time-consuming measurement procedure and to low time resolution. Costs and low time response hinder the application of GC in future large scale SOFC projects.

An alternative method is the Fourier Transform Infrared spectroscopy. It is absorption spectroscopy and is used to analyse oscillation spectra due to changes in the dipole moment during vibrations. The energy of the IR radiation is equal to the change in oscillatory levels, and the transitions are accompanied by changes in the quantum number of oscillations. To obtain the spectrum in the frequency domain from the spectrum measured by the interferometer, it is necessary to apply Fourier transform [35]. Thanks to the use of the adapter dedicated to a specific type of samples, it is possible to measure solids, liquids and gases with FTIR. The main advantages of FTIR over other techniques are the high selectivity achieved thanks to high resolution measurements as well as the possibility to simultaneously measure the content of many substances. Another advantage is the high sensitivity that allows the measurement of components at really small concentrations. Due to their construction, FTIR spectrometers allow

to significantly increase the signal-to-noise ratio by averaging interferograms from multiple spectral scanning. Besides, FTIR offers the possibility of continuous measurement "in situ" during the operation of the fuel cell, which is very hard with other measurement methods. Thanks to these advantages, this method has been used in this study.

To quantitatively determine a composition of investigated substance using FTIR, e.g. an unknown concentration of a gas mixture [36-38], it is required to perform a calibration procedure at the beginning of the experiment. It assumes that the size of FTIR absorbance peaks can be directly related to a concentration of the investigated substance. An exemplary comparison of FTIR absorbance peaks for different concentrations of CO_2 is shown in Fig.1.

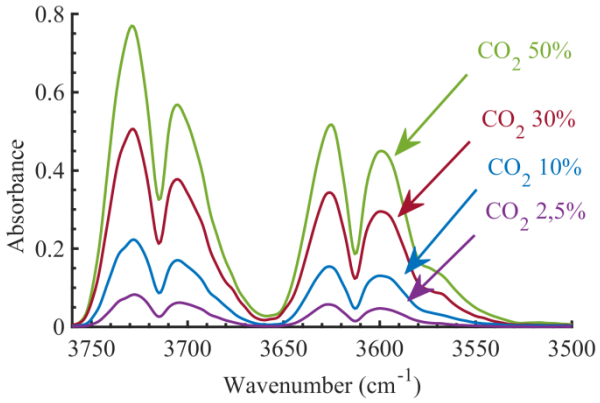

Fig. 1: The FTIR spectra of CO_2 with different concentration.

Generally FTIR analysis bases on the Beer-Lambert law, which relates the light absorption to the material properties and indicates a linear dependence between the absorbance and a substance concentration, but in practice, it is fulfilled only for dilute solutions. At concentrations exceeding about 0.01 M, the average distances between ions or molecules of the absorbing sample are diminished to the point where each particle affects the charge distribution of its neighbours. The occurrence of this phenomenon causes deviations from the linear relationship between absorbance and concentration [39]. Moreover, there are also some technical limitations caused mainly by the relatively low spectral setting of the instrument (in our experiment 4 cm^{-1} which is a compromise between high scan speed and a reasonable resolution) compared to the molecular spectral line-width of the measured gases (≈0.1 cm^{-1}) [40]. Therefore, a calibration procedure should be performed at the beginning of the experiment. As reported by Bak and Larsen [40], the observed nonlinearity can be modelled by a specific chemometric method. Among quantitative methods, the most precise are the multivariate techniques based on response at several wavenumbers. Such an approach gives a high signal-to-noise ratio. However, for concentrations above 0.5 vol.% of measured gases, the univariate techniques are sufficient and give satisfactory results. In general, they rely on modelling the relationship between absorbance values and concentrations by peak heights of the spectral lines or the integrated absorbances of the entire band. Bak and Larsen [40] found that the relation between the absorbance and concentration values for CO has the same functional form for the integrated absorbance calculated in a selected wavenumber region as the absorbance at a single wavenumber. Therefore both approaches are acceptable. However, the one with integrated absorbance performs better in the low concentration limit, because a sum of absorbance values over several wavenumbers is less sensitive to noise. Moreover, due to a higher sensitivity to a baseline shift in calculations at a single wavenumber, an approach with absorbance integration in selected wavenumber regions is recommended.

Therefore, in this paper the integrated absorbance areas were calculated in determined wavenumber ranges according to Eq.12:

$$I = \int_{\tilde{\nu}_1}^{\tilde{\nu}_2} A(\tilde{\nu}) d\tilde{\nu} \qquad (12)$$

where A is the measured absorbance, I the integral value, $\tilde{\nu}_1$ and $\tilde{\nu}_2$ are the wavenumber ranges for integration.

The objective of this work was to develop a method to analyse a composition of outlet gases from a DIR-SOFC fuelled by synthetic biogas. These measurements performed continuously during SOFC operation, allow investigating a process of internal reforming of hydrocarbons. Combined with results of electrical measurements

allow better understanding a degradation of a fuel cell and predicting a predominance of particular reforming reactions depending on conditions in a fuel cell chamber at a particular time.

2. Experimental

2.1. Calibration

In the calibration procedure, the system shown in Fig. 2 was used. The calibration mixture was composed of a dilution gas (Ar) mixed with CO_2, CO or CH_4. The concentration of these gases was varied using two mass flow meters. Such setup allowed obtaining particular calibration points.

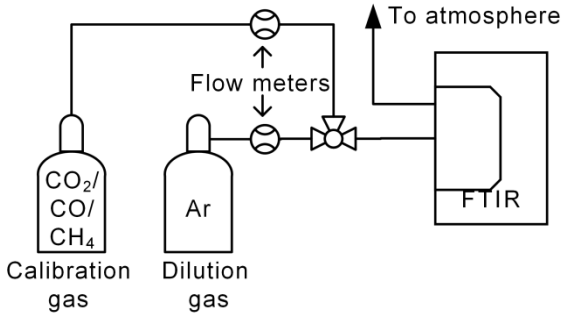

Fig. 2: Schematic view of the system used to obtain calibration curves.

The resulting mixture was delivered directly to the FTIR cell. The measurement was carried out using the PerkinElmer Spectrum 100 spectrometer with a 10 cm path length gas cell and ZnSe windows. The spectra were collected at 4 cm^{-1} resolution. At the beginning of the investigation, the FTIR cell was purged with argon. Then the desired mixture of gases with a total flow of 30 ml/min was supplied to FTIR for 10 minutes in order to reach a stable gas composition. Next, ten spectrograms were collected at every 2 minutes. The procedure was repeated for CO, CO_2 and CH_4 gases (of a concentration up to 70%). Graphical summary of this procedure is shown in supplementary materials (Fig.S1 left).

For the calculations of integrated absorbance, the peaks that do not change its shape with increasing concentration were chosen. Additionally, if the compound had several peaks, the ones that do not overlap with H_2O bands and with other measured gases were preferred. The selected wavenumber ranges were: 3760-3520 cm^{-1} for CO_2, 2226-2143 cm^{-1} for CO, 3250-2650 cm^{-1} for CH_4. They are depicted by vertical dashed lines in an FTIR spectrum of biogas shown in Fig.3. Although hydrogen was not visible in FTIR spectra, its concentration was calculated as a difference between 100% and a sum of concentrations of CO_2, CO and CH_4. The water was not present in a gas mixture, because it was trapped in a water condensing unit installed before the FTIR inlet.

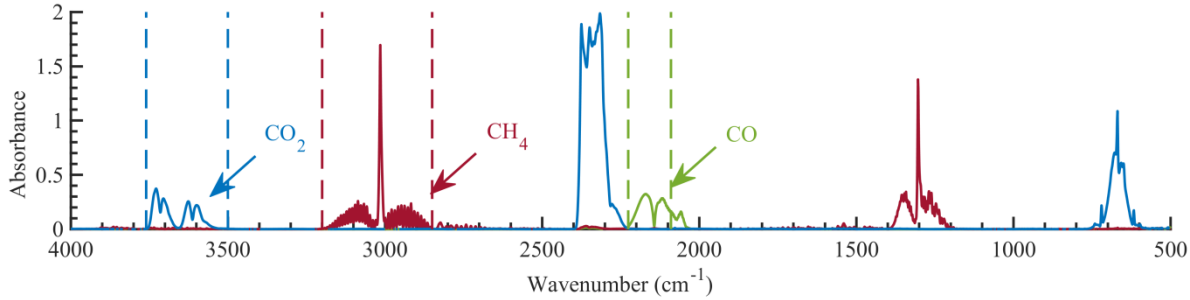

Fig. 3: The FTIR spectrum of biogas. Vertical dashed lines mark the wavenumber ranges used for quantitative analysis of particular gases.

2.2. SOFC measurements system

To measure the composition of outlet gases from SOFC, a system was modified. A scheme of this system is presented in Fig. 4.

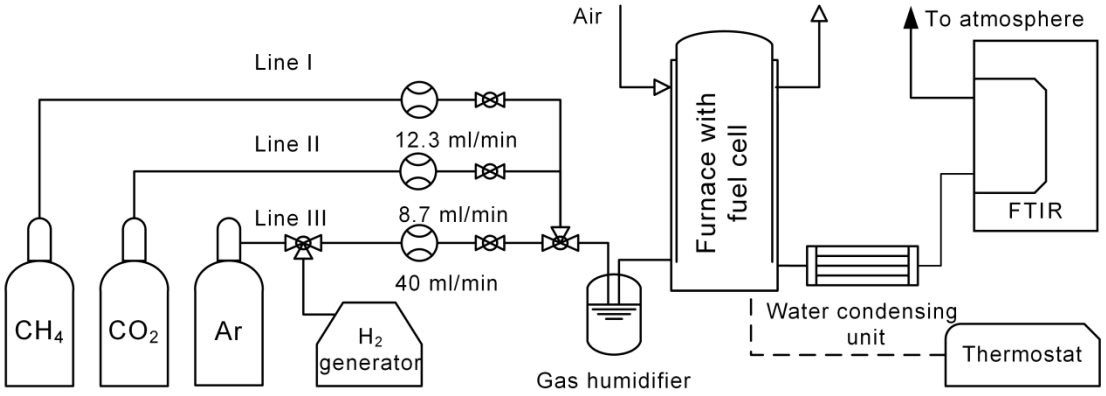

Fig. 4: Schematic view of the system for quantitative analysis of outlet gases from SOFC.

The fuel cell was fed with synthetic biogas which was a mixture of CO_2 (Linde, N5.0) and CH_4 (Linde, N5.5) in a volume ratio 2:3 with the addition of approximately 3% of water. Water concentration was controlled by feeding dry fuel through a gas humidifier kept at a constant temperature 23°C and pressure 1 atm. Its value was calculated according to the Antoine equitation for a steam (Eq. 13) [41].

$$\log p_{sat}[bar] = 3.56 - \frac{1838.68}{T[K] - 31.74} \quad (13)$$

Gases forming synthetic biogas were supplied using the line I and II. Line III was used to supply interchangeably neutral gas (Ar) or H_2 as a fuel. The flow of each gas was controlled by a corresponding mass flow meter. The inlet gases were always passing through the humidifier, and then they were directed to the measurement rig presented in Fig. 5. The temperature was controlled by a thermocouple placed beside a fuel cell. The fuel cell was spring loaded to the alumina tube and sealed by a silver paste preventing gas leakage from the anode side.

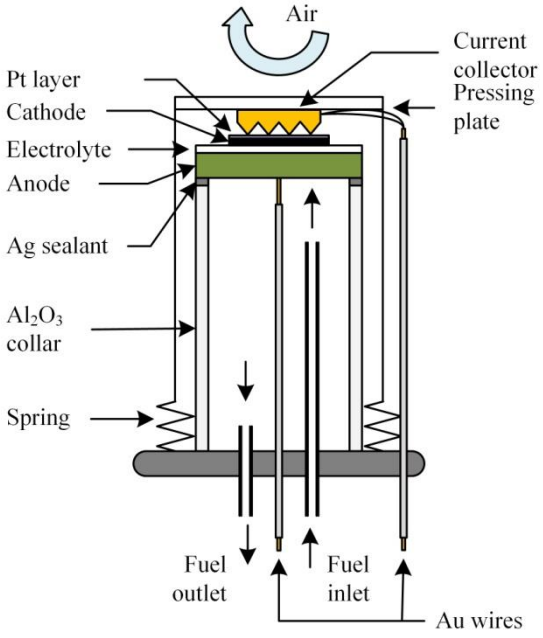

Fig. 5: Measurement rig for SOFC investigations, adapted from [2].

The concentration of gases determined from FTIR data allowed calculating other catalytic parameters: the conversion rates X of CH_4 and CO_2 (Eqs. 14 and 15, respectively), the selectivities S of CO and H_2 (Eqs.16 and 17, respectively) and the yields Y of CO and H_2 (Eqs. 18 and 19 respectively).

$$X_{CH_4} = \frac{n_{inCH_4} - n_{outCH_4}}{n_{inCH_4}} \cdot 100\% \quad (14)$$

$$X_{CO_2} = \frac{n_{inCO_2} - n_{outCO_2}}{n_{inCO_2}} \cdot 100\% \quad (15)$$

$$S_{CO} = \frac{n_{outCO}}{\left(n_{inCH_4} - n_{outCH_4}\right) + \left(n_{inCO_2} - n_{outCO_2}\right)} \cdot 100\% \quad (16)$$

$$S_{H_2} = \frac{n_{outH_2}}{2\left(n_{inCH_4} - n_{outCH_4}\right)} \cdot 100\% \quad (17)$$

$$Y_{CO} = \frac{n_{outCO}}{n_{inCO_2} + n_{inCH_4}} \cdot 100\% \quad (18)$$

$$Y_{H_2} = \frac{n_{outH_2}}{n_{inH_2O} + 2n_{inCH_4}} \cdot 100\% \quad (19)$$

where $n_{inCH_4}, n_{inCO_2}, n_{inH_2O}$ and $n_{outCH_4}, n_{outCO_2}, n_{outCO}, n_{outH_2}$ are the inlet and outlet molar concentrations of respective gases. X, S and Y are expressed in percentages. Conversion (X) gives us an information about how much of an initial fuel was utilized in a fuel cell chamber (both within reforming and electrochemical processes). The yield (Y) parameter shows how much of a desired product (CO or H_2) was found in the outlet stream with respect to the theoretical amount calculated from the chemical reactions, whereas selectivity (S) indicates how much of desired product was formed in ratio to the utilized fuel. All calculations have been done assuming that no leakage of inlet or exhaust gases was present.

Moreover, the carbon balance in time was determined as an average rate of carbon deposition during dwell time. It was calculated as a difference between the moles of carbon in the inlet and the outlet stream of gases (Eq.20):

$$C_{balance}(t) = n_{inCH_4} + n_{inCO_2} - n_{outCH_4} - n_{outCO_2} - n_{outCO} \quad (20)$$

The electrical properties of the fuel cell were measured using the HAMEG 8143 power supply. Gold wires, which do not act as reforming catalysts, were connected to the anode side. The cathode was coated with a platinum interconnector to improve the connection with a current collector. Then it was spring loaded by a gold covered alumina grating, which allowed free flow of atmospheric air to the cathode site.

Due to strong IR bands of water in a measured wavelength range, the outlet gas was dehumidified using condensing unit set (water trap) operating at 3°C. Then, outlet gases were transferred to the FTIR cell. FTIR data was collected by the Spectrum™ TimeBase software. Additionally, an application was created in the MATLAB™ environment to facilitate the analysis of gathered FTIR data. During prolonged measurements (above 5 h) spectra baseline deterioration was observed. To correct this error, an additional baseline correction Savitzky-Golay filter was used before all calculations [42,43].

2.3. Measurement procedure

The investigated 1-inch anode supported SOFC was fabricated as described in our previous paper [44] and consisted of Ni-YSZ anode, YSZ electrolyte and LSM-YSZ cathode (of surface area 1.13 cm^2). Two types of electrical measurements were performed: a current density versus voltage measured every 24 h and a current density versus time under a constant load of 0.65 V collected every 0.5 min. FTIR spectra were collected every 10 min.

Flowchart of SOFC operation and data gathering procedure is shown in supplementary materials (Fig.S1 right). Initially, the fuel cell was slowly (3°C/min) heated up to 800°C in an argon atmosphere. Afterwards, a nickel oxide was reduced to a metallic form in 40 ml/min hydrogen flow for 30 min. Next, the temperature was decreased down to 750°C, and the fuel cell was operating for 24 h with pure hydrogen fuel. The current density was measured for a reference. Further, hydrogen was replaced by synthetic biogas with 3% steam, which flow was set to 21 ml/min. The fuel cell was operating in biogas for 96 h. During this step, the current density and FTIR spectra of outlet gases were measured.

2.4. Chemical equilibrium analysis and carbon activity coefficient

Due to water removal from measured output mixture (it was trapped in a water condensing unit installed before the FTIR inlet), its amount was estimated according to a mass-atom balance of hydrogen and oxygen. It

was assumed, that from every two unbalanced atoms of hydrogen and one unbalanced atom of oxygen one molecule of water is formed.

An amount of unbalanced H and O atoms was calculated as a difference between the moles of these elements in the inlet and the outlet stream of gases. Moreover, the additional source of oxygen were oxygen ions pumped during SOFC operation through electrolyte into the anode reaction area in order to oxidize i.e. CO, CH_4 and H_2. The total flux of these oxygen ions ($n_{O^{2-}}$) was calculated from the Faraday equation (21) and also taken for mass-atom balance calculations:

$$n_{O^{2-}} = \frac{S}{2N_A e}\int j(t)dt \quad (21)$$

where j(t) is a current density measured at a particular time, and S is an active cathode area.

Therefore general formulae for calculations of unbalanced H and O atoms are represented by (Eq.22) and (Eq.23) respectively:

$$\Delta H = 4n_{inCH_4} + 2n_{inH_2O} - 4n_{outCH_4} - 2n_{outH_2} \quad (22)$$

$$\Delta O = n_{O^{2-}} + n_{inH_2O} + 2n_{inCO_2} - 2n_{outCO_2} - n_{outCO} \quad (23)$$

The calculated amount of unbalanced H and O atoms was concerned to form water molecules removed before FTIR analysis. Estimation of water amount was undertaken to provide information for further non-equilibrium analysis in order to predict the direction of particular reforming reactions.

Several approaches concerning equilibrium calculations for methane reforming were already mentioned in other publications [45-48]. In order to determine the behaviour of each from series of mentioned reactions, a time-dependent thermodynamic analysis was performed using reaction quotients (Q_r) [45,46,49], which represent a ratio between an actual non-equilibrium constant and equilibrium constant of a specific reaction. Q_r value aids in figuring out the momentary direction in which reactions are likely to proceed. Mathematically Q_r is calculated from Eq.24 as a ratio of actual overall partial pressures p_i of species "i" raised to the power of stoichiometric coefficient x_i (positive for products and negative for reactants) and equilibrium constant $K_{p,r}$ of discussed reaction. Each of the mentioned reactions was taken into account separately for Q_r value estimation in order to simplify the calculation method while providing sufficient enough data for further analysis of equilibrium shifting. All theoretical equilibrium constants K_p were taken from the HSC Chemistry software.

$$Q_{r_{(t)}} = \frac{(\prod_i {p_{i_{(t)}}}^{x_i})_r}{K_{p,r}} \quad (24)$$

Quotient indicates if the mentioned reaction goes to the right (for Q_r<1) or to the left (for Q_r>1). When Q_r=1 reaction has reached an equilibrium point. It is commonly approved that $Q_r \sim 10^{-3}$ stands for the situation when mostly reactants are present in reaction area, while $Q_r \sim 10^{3}$ when nearly all substances are products and finally if $10^{-3} < Q_r < 10^{3}$ then significant amounts of both reactants and products are visible [50].

In order to analyse a carbon deposition process reactions (8), (9) and (10) can be described additionally by carbon activity coefficient $\alpha_{C,r}$, which is a reciprocal of Q_r and can be calculated according to Eq. 25.

$$\alpha_{C,r} = Q_r^{-1} \quad (25)$$

Parameter $\alpha_{C,r}$ defines whether carbon formation is thermodynamically possible. It is generally accepted that carbon activity coefficient equals 1 at equilibrium. In case when $\alpha_{C,r}$>1 solid carbon formation is promoted [49,51]. Values of coefficient $\alpha_{C,r}$ were used to describe how specific reaction influences the coking process.

3. Results and discussion

3.1. Calibration curves

Fig. 6-8 show the calibration curves obtained for CO_2, CO and CH_4, respectively. In these figures also the polynomial functions modelling the relationship between the concentrations (C) of particular gases and the integrated absorbance (A) calculated in selected wavenumber regions both with the coefficients of determination (R^2) are presented. All curves show nonlinear deviation from the Beer-Lambert law. The 3rd order polynomials expressed the C(A) relationships for all CO_2, CO and CH_4 gases. Such high polynomial orders are in agreement with literature reports. Bak and Larsen [40] performed a calibration procedure for CO gas and found that even a 5th polynomial gave a sufficiently high degree of accuracy in the relation between the concentrations of the calibration gas against the integrated absorbance C(A).

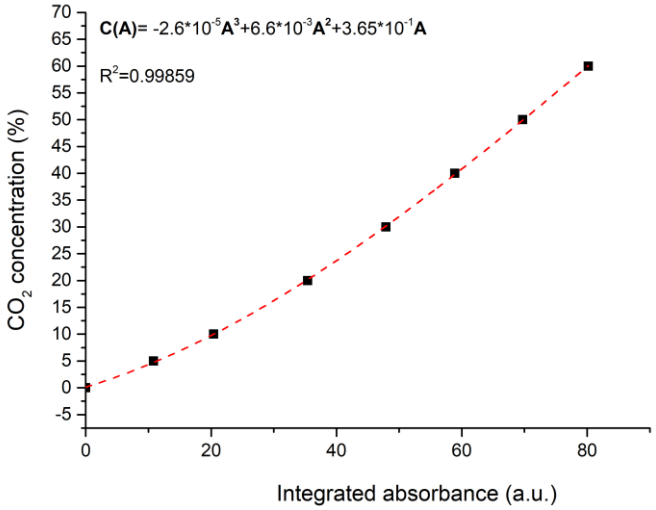

Fig. 6: Calibration curve for CO_2 within 3760-3520 cm^{-1} wavenumber range.

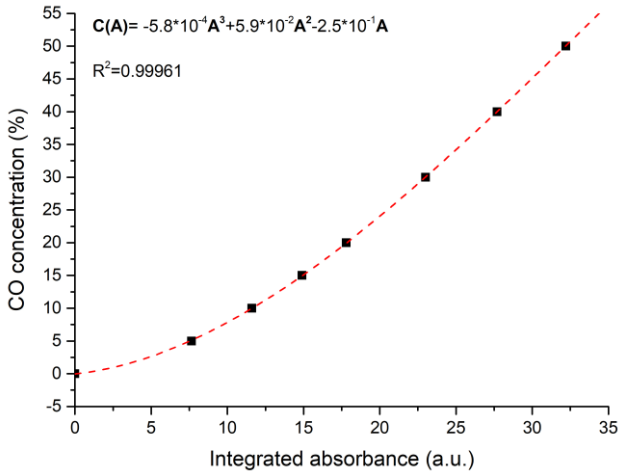

Fig. 7: Calibration curve for CO within 2226-2143 cm^{-1} wavenumber range.

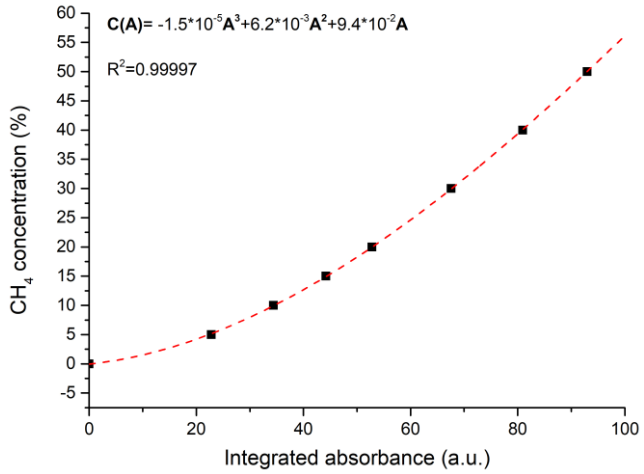

Fig. 8: Calibration curve for CH_4 within 3250-2650cm^{-1} wavenumber range.

3.2. Electrical tests and analysis of SOFC outlet gases

The investigation of long-term electrical stability was performed during initial SOFC feeding with hydrogen (for 30 h) and further with biogas (for 90 h). The obtained results are presented in Fig.9a as a plot of current density vs time and in Fig.10 as the I-V curves. The moments in which the I-V measurements were carried out are marked in Fig.9a. The obtained results indicate that when the SOFC was fuelled by hydrogen, its current density, as well as a maximum power density increased due to an ongoing nickel reduction process. After 10-15 h the stable current density was obtained. Sometimes, once a maximum current density is reached, a further decrease of this parameter may be observed [52]. This may be explained by e.g. ordering of metallic nickel in the structure of the anode or the segregation of impurities. However, it has not been observed in this investigation. The OCV values measured both at the beginning and at the end of the operation in hydrogen were equal to 1.02 V, which is slightly lower than the theoretical value predicted by the Nernst equation.

In the next step, the fuel supplied to the SOFC anode site was switched to synthetic biogas. As a result, a rapid current density drop of *ca.* 10% was noticed. Then, during the first 12 h of operation in biogas, a further decrease (5%) of current density was observed. After this time a system stabilized and no significant changes of current density were observed till the 65th hour of biogas supplying. Since then a further current density decrease began, which became significantly rapid after 75 h of biogas feeding. The total decrease in current density compared to hydrogen was 20% after 90 h of operation in biogas fuel. The OCV value measured after this time was also lower (~1 V) than in hydrogen. Since not only electrochemical oxidation of hydrogen (Eq.4) is possible in the system, but also CO, CH_4 and solid carbon can be oxidized (Eqs. 6,7,11), the theoretical OCV in biogas is a combination of the different reactions taking place at the anode surface and it might be different than in pure hydrogen [53,54]. However, a decrease of OCV comes rather from H_2 dilution within CO_2, CO and CH_4 gases. It correlates well with a decrease of CH_4 and CO_2 conversion rates (less fuel is utilized) in time and is in agreement with literature reports. Hagen et al. also found [55] that OCV for the biogas fueled SOFC decreased when more inlet fuel passed unconverted through the SOFC as a result of H_2S poisoning.

An analysis of outlet gases composition was also performed simultaneously with the electrical measurements. A plot presenting concentration of CH_4, CO_2, CO and H_2 gases as a function of time is shown in Fig.9b. It indicates that at the beginning (first 12 hours of operation in biogas) an initial biogas mixture (58 vol.% of CH_4, 39 vol.% of CO_2 and 3 vol.% of H_2O) is partially converted into CO and H_2, whereas an amount of unconverted gases increases (to 27% for CH_4 and to 21% for CO_2). This increase leads to a slight decrease of reforming products amount which acts as a direct fuel for SOFC and correlates well with a decrease of current density shown in Fig.9a. Within the next 20 hours (from 12 to 32h) one can see a further increase of non-reacted methane which is correlated with a simultaneous depletion of CO in exhaust gases mixture. An amount of carbon dioxide and hydrogen remains almost constant in that period of time. After 42 hours of operation in biogas, a concentration of CH_4 in the outlet stream starts to exceed an amount of produced H_2. Also a concentration of CO decreases in time as well as the amount of not utilized CO_2 increases allowing to conclude that reforming process becomes less and less efficient. However, no significant changes can be found in the current density plot (Fig.9a) at this time. After 65 hours of operation in biogas, a concentration of CO and CO_2 in the outlet stream stabilizes (~24% for CO_2 and ~20% for CO).

The observed change of gases concentrations leads to a change of reforming parameters (conversion, yield, selectivity) shown in Fig.9c. Both CO_2 and CH_4 conversions decrease in a whole time of operation in biogas indicating that less and less fuel is utilized in a fuel cell chamber (both within reforming and electrochemical processes). Within a whole time of analysis, the conversion of CH_4 is higher than that of CO_2. Two other parameters, the yield of CO and H_2, also decrease as a function of time. Only after 65 hours of operation in biogas they become almost constant, but at the end of the measurement, both of them are quite low (~20%). Finally, the selectivities of H_2 and CO are quite stable in time. Although between 12th and 46th hour of biogas feeding one can see a kind of instability (CO selectivity decreases, H_2 selectivity increases), but after 65 hours both these parameters become constant and equal to 43%.

Both yields and selectivities refer to the amount of the desired product (CO or H_2) that was found in the outlet stream. However, one should realize that CO and H_2 concentrations taken for the calculations are the products which were not consumed in the electrochemical reactions. If more hydrogen is utilized within electrochemical oxidation according to the reaction (5), then less hydrogen will be found in the outlet stream and one will obtain lower H_2 yield.

However, despite changes in the reforming parameters, the current density between 12th and 75th hour of biogas supplying is almost constant. ~~Therefore few hypotheses are possible to explain these differences. The first one suggests that a dominant electrochemical reaction is CO oxidation (5) and thus an almost constant CO concentration corresponds well with a constant current density in time. But since a rate of electrochemical oxidation of H_2 is considerably faster than that of CO, the H_2 concentration may be the key factor influencing the~~

~~electrochemical performance. The other possibility is that the changes in the ongoing electrochemical processes may compensate each other (an increase of CO oxidation may compensate any decrease in H_2 oxidation). The last hypothesis~~ It suggests that the amount of H_2 and CO gases consumed within electrochemical oxidation remains constant. According to literature reports [56,57], these reactions (Eq.5 and 6) are supposed to be faster than the reforming reactions. Therefore they will occur as long as the fuel composition does not change significantly. However, one should remember that the hydrogen and carbon oxide found in the outlet stream is a non-utilized fuel which was not consumed in the electrochemical reactions. Even if the amount of hydrogen decreased in the outlet stream, its amount taken for reaction (5) could have been unchanged.

Interestingly, when almost all reforming parameters stabilize (after 65 h), a current density starts to decrease. It may suggest that an anode structure could have been changed (e.g. due to coking) and a triple phase boundary could have been shortened. Then less active sites are accessible and the electrochemical performance of SOFC decreases.

To sum up these divagations, it can be concluded that an internal reforming of biogas during SOFC operation is a very complex process realized by various phenomena taking place simultaneously. It is influenced by many factors, such as anode microstructure, gas composition, temperature, external current load, humidity of gas etc. Moreover, among possible reforming reactions occurring in particular conditions, some of them may be shifted towards products and some towards reactants. In order to predict the direction of particular reforming reactions, a non-equilibrium analysis was performed. The results are shown and discussed in the next section.

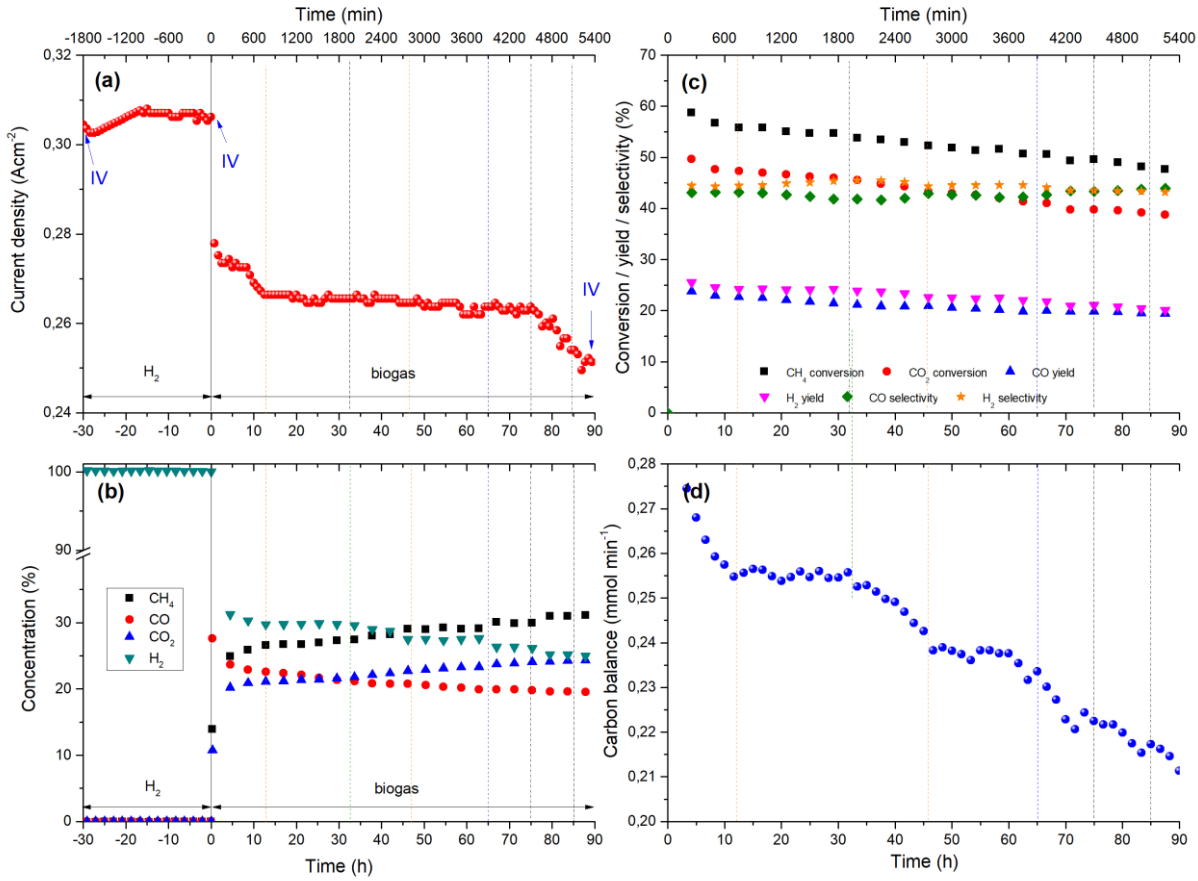

Fig.9: (a) Current density as a function of time and (b) composition of outlet gases from SOFC fuelled by hydrogen and further by biogas at 750 °C; (c) Conversion rates of CH_4 and CO_2, selectivities of CO and H_2, yields of CO and H_2 and (d) carbon balance as a function of time during SOFC operation in biogas at 750 °C.

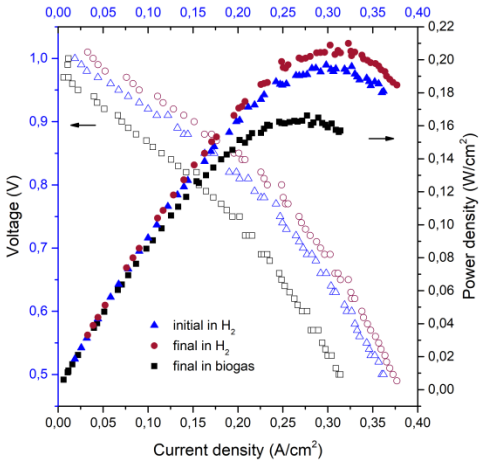

Fig. 10: The current density versus voltage (I–V) and current density versus power density (I–P) curves for SOFC at 750°C. The moments in which the I-V measurements were carried out are marked in Fig.9a.

3.3. Reaction equilibrium and carbon deposition process analysis

Non-equilibrium analysis of methane reforming reactions was performed using collected concentrations of exhaust gases. Time-dependent changes in Q_r values are presented in Fig. 11 and describe how much given reaction is away from its equilibrium. It can be seen that both dry and steam assisted reforming reactions are shifted towards products. In case of working fuel cell, mentioned reactions will provide methane decomposition into H_2 molecules, while steam reforming is much more favourable concerning the existence of an observable amount of water in reaction atmosphere. Reverse water-gas shift reaction shows high reaction rate as it fast reaches equilibrium composition regions. It has been described in the literature [58] that RWGS has a near equilibrium composition of reactants and products in a wide range of temperatures and assumed that this reaction is at equilibrium point in the kinetic treatment. By this fact one can say that it has a secondary meaning in hydrogen production [58]. Methanation reaction can be considered fully shifted towards reactants and taking part in CH_4 decomposition.

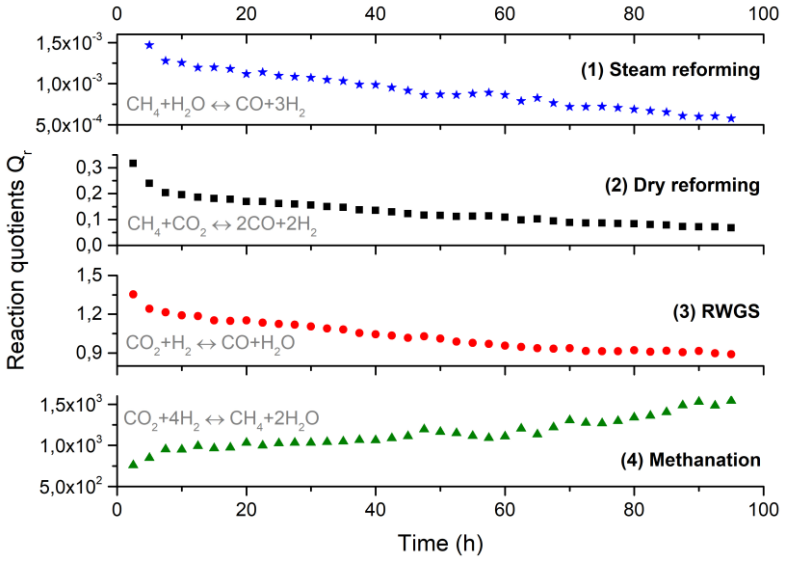

Fig.11: Time dependence of reaction quotients (Q_r) for steam reforming, dry reforming, reverse water gas-shift (RWGS) and methanation reactions.

The analysis of reactions responsible for solid carbon (Eq. 8-10) formation is depicted in Fig. 12 as values of calculated carbon activity coefficients $\alpha_{C,r}$ at particular periods of time. Among them, only $\alpha_{C,r}$ for methane pyrolysis reaction is significantly higher than unity. Therefore, it can be concluded that methane cracking is the main reason for fuel cell coking considering chosen fuel mixture composition, working parameters and a type of

SOFC. In two other cases, reactions proceed rather towards reactants, which implies that those do not promote carbon accumulation ($\alpha_{C,r}$ <1). Taking into account a carbon balance plot (Fig.9d) it can be seen that the carbon deposition rate strongly depends on the gas composition and changes slightly within working time. Apart from solid carbon being a product of reforming reactions, one should also consider a decrease of anode's specific surface, which additionally limits carbon formation. Moreover, a part of solid carbon is electrochemically oxidized, because the flux of oxygen ions under the fuel cell operation the closed-circuit condition is fast enough to remove coke deposition [56]. Therefore, in order to prevent electrode coking, various factors, such as inlet gas composition, working temperature, current load and anode's functional layers need to be optimized.

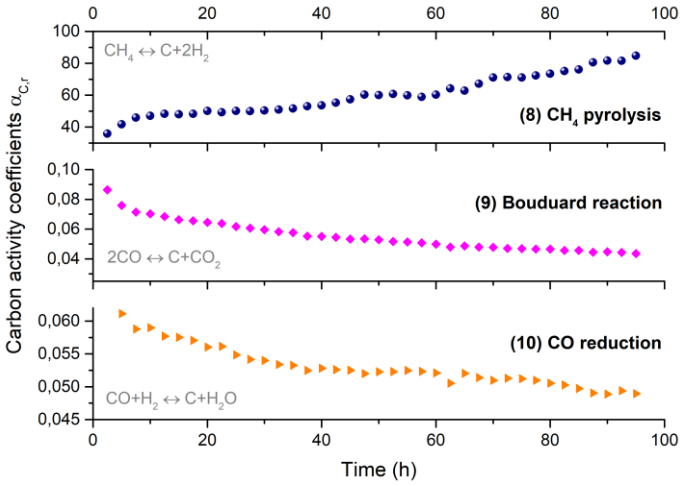

Fig.12: Time dependence of carbon activity coefficients (α_c) for CH_4 pyrolysis, CO reduction and Bouduard reactions.

4. Conclusions

In this study, the Fourier Transform Infrared Spectroscopy for the in-situ, quantitative analysis of the composition of outlet gases from Solid Oxide Fuel Cell (SOFC) was described. The calibration procedure performed at the beginning of the experiment indicated a polynomial dependence between the concentration of a calibrating gas (CO, CO_2, CH_4) and the corresponding integrated absorbance in particular wavenumber ranges. Further, it allowed concentration determination of CO_2, CO, CH_4 and H_2 in the outlet gas stream coming from the Ni–YSZ anode supported DIR-SOFC fuelled by synthetic biogas (mixture of CO_2 and CH_4 in a volume ratio 2:3) for over 90 hours.

A constant increase in the amount of non-reacted fuel (CH_4 and CO_2) together with a decrease of reforming products (CO and H_2) was observed during operation, confirming a decrease in the direct internal reforming process. Although both the conversion parameters of CO_2 and CH_4, as well as the yields of H_2 and CO decreased, the selectivities of both CO and H_2 remained almost constant in time.

Basing on a comparison between a current density plot and the concentration/yield/selectivity of gases it was suggested that the H_2 concentration might be the key factor influencing the electrochemical performance. Current density may remain constant as long as the fuel composition does not change significantly or as long as the changes in the ongoing electrochemical processes may compensate each other (an increase of CO oxidation may compensate any decrease in H_2 oxidation). It was also concluded that the internal reforming of biogas during SOFC operation is a very complex process dependent on various phenomena taking place simultaneously. It is influenced by many factors, such as anode microstructure, gas composition, temperature, external current load, humidity of gas etc.

From a non-equilibrium analysis, it was found that a steam reforming of methane is the most favourable direct internal reforming reaction due to the existence of the observable amount of water in a reaction atmosphere. On the other hand, methanation reaction is considered fully shifted towards reactants and taking part in CH_4 decomposition. Among reactions leading to carbon deposition, the CH_4 pyrolysis seems to be a dominant one, because the carbon activity coefficient of this process was few orders of magnitude higher than for other reactions.

Finally, it can be stated that applied FTIR quantitative method has proven to be reliable, with consistent results. It suggests that this analysis can be applied for investigation of SOFC fuelled by any gases (e.g. also by H_2S contaminated biogas). The only requirement is to perform a suitable calibration process for particular gas previously. The gas parameters (concentration/conversion/yield/selectivity) in correlation with an analysis of

reaction quotients and measurements of electrical properties gives additional information about the process of biogas reforming taking place on the anode side of the SOFC.

Acknowledgement

Authors would like to acknowledge Mr Oskar Białk for his help in the calibration procedure. This work was financially supported by the National Science Centre under grant No. NCN 2017/26/D/ST8/00822.

Reference

[1] Abdalla AM, Hossain S, Azad AT, Petra PMI, Begum F, Eriksson SG, et al. Nanomaterials for solid oxide fuel cells: A review. Renew Sustain Energy Rev 2018;82:353–68. doi:10.1016/j.rser.2017.09.046.

[2] Szymczewska D, Karczewski J, Bochentyn B, Chrzan A, Gazda M, Jasiński P. Investigation of catalytic layers on anode for solid oxide fuel cells operating with synthetic biogas. Solid State Ionics 2015;271:109–15. doi:10.1016/j.ssi.2014.10.023.

[3] Chiba R, Taguchi H, Komatsu T, Orui H, Nozawa K, Arai H. High temperature properties of $Ce_{1-x}Pr_xO_{2-\delta}$ as an active layer material for SOFC cathodes. Solid State Ionics 2011;197:42–8. doi:10.1016/J.SSI.2011.03.022.

[4] Taguchi H, Chiba R, Komatsu T, Orui H, Watanabe K, Hayashi K. LNF SOFC cathodes with active layer using Pr_6O_{11}or Pr-doped CeO_2. J Power Sources 2013;241:768–75. doi:10.1016/j.jpowsour.2013.04.141.

[5] Alvarado Flores JJ, Ávalos Rodríguez ML, Andrade Espinosa G, Alcaraz Vera JV. Advances in the development of titanates for anodes in SOFC. Int J Hydrogen Energy 2018. doi:10.1016/j.ijhydene.2018.05.171.

[6] Dzul, I., Hernández, T., Hernández Carrillo, R. et al. Synthesis and electric properties of perovskite $Pr_{0.6}Ca_{0.4}Fe_{0.8}Co_{0.2}O_3$ for SOFC applications. Ionics 2014;20:1031. doi.org/10.1007/s11581-014-1150-z

[7] Bicer Y, Khalid F. Life cycle environmental impact comparison of solid oxide fuel cells fueled by natural gas, hydrogen, ammonia and methanol for combined heat and power generation. Int J Hydrogen Energy 2018, In press, doi.org/10.1016/j.ijhydene.2018.11.122

[8] Lee HS, Lee HM, Park J-Y, Lim H-T, Degradation behavior of Ni-YSZ anode-supported solid oxide fuel cell (SOFC) as a function of H2S concentration, Int J Hydrogen Energy 2018; 43:22511-22518, doi.org/10.1016/j.ijhydene.2018.09.189

[9] Hernández SP, Scarpa F, Fino D, Conti R. Biogas purification for MCFC application. Int J Hydrogen Energy 2011;36:8112–8. doi:10.1016/j.ijhydene.2011.01.055.

[10] Cigolotti V, McPhail S, Moreno A, Yoon SP, Han JH, Nam SW, et al. MCFC fed with biogas: Experimental investigation of sulphur poisoning using impedance spectroscopy. Int. J. Hydrogen Energy, vol. 36, Pergamon; 2011, p. 10311–8. doi:10.1016/j.ijhydene.2010.09.100.

[11] Dicks A. Advances in catalysts for internal reforming in high temperature fuel cells. J Power Sources 1998;71:111–22. doi:10.1016/S0378-7753(97)02753-5.

[12] Lindkvist E, Karlsson M. Biogas production plants; existing classifications and proposed categories. J Clean Prod 2017;174:1588–97. doi:10.1016/j.jclepro.2017.10.317.

[13] Lackey J, Champagne P, Peppley B. Use of wastewater treatment plant biogas for the operation of Solid Oxide Fuel Cells (SOFCs). J Environ Manage 2017;203:753–9. doi:10.1016/j.jenvman.2016.09.006.

[14] Singhal SC, Kendall K. High-temperature solid oxide fuel cells: fundamentals, design, and applicatons. 2003. doi:10.1016/B978-185617387-2/50021-0.

[15] Sarno C, Luisetto I, Zurlo F, Licoccia S, Di Bartolomeo E, Lanthanum chromite based composite anodes for dry reforming of methane, Int J Hydrogen Energy 2018; 43: doi.org/10.1016/j.ijhydene.2018.06.021

[16] Yao X, Fan L, Gan T, Hou N, Li P, Zhao Y, Li Y, Coking-resistant NbO_x-Ni-$Ce_{0.8}Sm_{0.2}O_{1.9}$ anode material for methanol-fueled solid oxide fuel cells, Int J Hydrogen Energy 2018; 43: 12748-12755

[17] Papurello D, Lanzini A, Tognana L, Silvestri S, Santarelli M. Waste to energy: Exploitation of biogas from organic waste in a 500 W_{el} solid oxide fuel cell (SOFC) stack. *Energy*, 2015; 85: 145-158. doi: 10.1016/j.energy.2015.03.093.

[18] Papurello D, Silvestri S, Tomasi L, Belcari I, Biasioli F, Santarelli M. Biowaste for SOFCs. Energy Procedia 2016;101:424–31. doi:10.1016/j.egypro.2016.11.054.

[19] Shiratori Y, Sakamoto M. Performance improvement of direct internal reforming solid oxide fuel cell fuelled by H2S-contaminated biogas with paper-structured catalyst technology. J Power Sources 2016;332:170–9. doi:10.1016/j.jpowsour.2016.09.095.

[20] Authayanun S, Pornjarungsak T, Prukpraipadung T, Saebea D, Arpornwichanop A. SOFC running on steam reforming of biogas : External and internal reforming 2016;1:173. doi:10.3303/CET1652061.

[21] Xu C, Zondlo JW, Gong M, Elizalde-Blancas F, Liu X, Celik IB. Tolerance tests of H2S-laden biogas fuel on solid oxide fuel cells. J Power Sources 2010;195:4583–92. doi:10.1016/j.jpowsour.2010.02.078.

[22] Chiodo V, Galvagno A, Lanzini A, Papurello D, Urbani F, Santarelli M, et al. Biogas reforming process investigation for SOFC application. Energy Convers Manag 2015;98:252–8. doi:10.1016/j.enconman.2015.03.113.

[23] Pichas C, Pomonis P, Petrakis D, Ladavos A. Kinetic study of the catalytic dry reforming of CH4 with CO2 over $La_{2-x}Sr_xNiO_4$ perovskite-type oxides. Appl Catal A Gen 2010;386:116–23. doi:10.1016/j.apcata.2010.07.043.

[24] Maček J, Novosel B, Marinšek M. Ni–YSZ SOFC anodes—Minimization of carbon deposition. J Eur Ceram Soc 2007;27:487–91. doi:10.1016/j.jeurceramsoc.2006.04.107.

[25] Sarruf BJM, Hong JE, Steinberger-Wilckens R, de Miranda PE V. CeO2–Co3O4–CuO anode for direct utilisation of methane or ethanol in solid oxide fuel cells. Int J Hydrogen Energy 2018;43:6340–51. doi:10.1016/j.ijhydene.2018.01.192.

[26] Dang-Long T, Quang-Tuyen T, Shiratori Y. Catalytic and electrochemical behaviour of solid oxide fuel cell operated with simulated-biogas mixtures. AIP Conf. Proc., vol. 1737, 2016, p. 060012. doi:10.1063/1.4949319.

[27] Finnerty CM, Coe NJ, Cunningham RH, Ormerod RM. Carbon formation on and deactivation of nickel-based/zirconia anodes in solid oxide fuel cells running on methane. Catal Today 1998;46:137–45. doi:10.1016/S0920-5861(98)00335-6.

[28] Alzate-Restrepo V, Hill JM. Carbon deposition on Ni/YSZ anodes exposed to CO/H2 feeds. J Power Sources 2010. doi:10.1016/j.jpowsour.2009.09.014.

[29] Kuhn J, Kesler O. Carbon deposition thresholds on nickel-based solid oxide fuel cell anodes I. Fuel utilization. J Power Sources 2015;277:443–54. doi:10.1016/j.jpowsour.2014.07.085.

[30] Larminie J, Dicks A. Fuel cell systems explained. 2003. doi:10.1002/9781118878330.

[31] Ihara M, Matsuda K, Sato H, Yokoyama C. Solid state fuel storage and utilization through reversible carbon deposition on an SOFC anode. Solid State Ionics, vol. 175, 2004, p. 51–4. doi:10.1016/j.ssi.2004.09.020.

[32] Santoni F, Silva Mosqueda DM, Pumiglia D, Viceconti E, Conti B, Boigues Muñoz C, et al. In-situ study of the gas-phase composition and temperature of an intermediate-temperature solid oxide fuel cell anode surface fed by reformate natural gas. J Power Sources 2017;370:36–44. doi:10.1016/j.jpowsour.2017.09.078.

[33] Conti B, Pumiglia D, Arato E, McPhail S, Bosio B, Santoni F. A 2-D model for Intermediate Temperature Solid Oxide Fuel Cells Preliminarily Validated on Local Values. Catalysts 2019;9:36. doi:10.3390/catal9010036.

[34] Boigues Muñoz C, Bosio B, Carlini M, McPhail SJ, Pumiglia D, Viceconti E, et al. SOFC Anode Process Characterization by Means of a Spot-Sampling Set-up for in-Operando Gas Analysis. ECS Trans 2017;75:1–8. doi:10.1149/07549.0001ecst.

[35] Stuart BH. Infrared Spectroscopy: Fundamentals and Applications. vol. 8. John Wiley & Sons; 2004. doi:10.1002/0470011149.

[36] Granada E, Eguía P, Vilan JA, Comesaña JA, Comesaña R. FTIR quantitative analysis technique for gases. Application in a biomass thermochemical process. *Renewable Energy* 2012, 41:416–421. doi: 10.1016/j. renene.2011.11.020.
[37] Speitel LC. Fourier Transform Infrared Analysis of Combustion Gases. J Fire Sci 2002;20:349–71. doi:10.1177/0734904102020005484.
[38] Marsanich K, Barontini F, Cozzani V, Petarca L. Advanced pulse calibration techniques for the quantitative analysis of TG ± FTIR data. Techniques 2002;390.
[39] Skoog DA, West DM, Holler FJ, Crouch SR. Fundamentals of analytical chemistry. Ninth Edit. Brooks/Cole, Cengage Learning; 2014.
[40] Bak J, Larsen A. Quantitative Gas Analysis with FT-IR: A Method for CO Calibration Using Partial Least-Squares with Linearized Data. Appl Spectrosc 2005;49:437–43. doi:10.1366/0003702953964237.
[41] Bridgeman OC, Aldrich EW. Vapor pressure tables for water. J Heat Transf 1964;86:279–86. doi:10.1115/1.3687121.
[42] Andrade L, Manolakos ES. Signal Background Estimation and Baseline Correction Algorithms for Accurate DNA Sequencing. J VLSI Signal Process Syst Signal Image Video Technol 2003;35:229–43. doi:10.1023/B:VLSI.0000003022.86639.1f.
[43] Zhao A. The parameters optimization selection of Savitzky-Golay filter and its application in smoothing pretreatment for FTIR spectra 2014.
[44] Wang S.F., Wang Y.R., Yeh C.T., Hsu Y.F., Chyou S.D., Lee W.T., Effects of bi-layer LSCF-based Cathodes on Characteristics of Intermediate Temperature SOFCs, Journal of Power Sources, 2011;196: 977-987
[45] Xu J, Froment GF. Methane steam reforming, methanation and water-gas shift: I. Intrinsic kinetics. AIChE J 1989;35:88–96. doi:10.1002/aic.690350109.
[46] Hou K, Hughes R. The kinetics of methane steam reforming over a Ni/α-Al2O catalyst. Chem Eng J 2001;82:311–28. doi:10.1016/S1385-8947(00)00367-3.
[47] Ginsburg JM, Piña J, El Solh T, De Lasa HI. Coke formation over a nickel catalyst under methane dry reforming conditions: Thermodynamic and kinetic models. Ind Eng Chem Res 2005;44:4846–54. doi:10.1021/ie0496333.
[48] Klein JM, Bultel Y, Georges S, Pons M. Modeling of a SOFC fuelled by methane: From direct internal reforming to gradual internal reforming. Chem Eng Sci 2007;62:1636–49. doi:10.1016/j.ces.2006.11.034.
[49] Jaworski Z, Zakrzewska B, Pianko-Oprych P. On thermodynamic equilibrium of carbon deposition from gaseous C-H-O mixtures: Updating for nanotubes. Rev Chem Eng 2017;33:217–35. doi:10.1515/revce-2016-0022.
[50] Petrucci, et al. General Chemistry Principles & Modern Applications. 9th ed. Upper Saddle River, NJ: Pearson Prentice Hall, 2007
[51] Tsiakaras P, Demin A. Thermodynamic analysis of a solid oxide fuel cell system fuelled by ethanol. J Power Sources 2001;102:210–7. doi:10.1016/S0378-7753(01)00803-5.
[52] Bochentyn B, Chlipała M, Gazda M, Wang SF, Jasiński P. Copper and cobalt co-doped ceria as an anode catalyst for DIR-SOFCs fueled by biogas. Solid State Ionics 2019;330:47–53. doi:10.1016/j.ssi.2018.12.007.
[53] Escudero M. J., Fuerte A., Electrochemical analysis of a system based on W and Ni combined with CeO_2 as potential sulphur-tolerant SOFC anode. Fuel Cells 2016,16,3:340–348
[54] Milewski J., The influence of fuel composition on Solid Oxide Fuel Cell obtained by using the advanced mathematical model, Journal of Power Technologies 2011;91(4): 179–185
[55] Hagen A, Winiwarter A, Langnickel H, Johnson, G, SOFC Operation with Real Biogas 2017 Fuel Cells, 17(6), 854-861. DOI: 10.1002/fuce.201700031
[56] Moon DJ, Ryu JW. Electrocatalytic reforming of carbon dioxide by methane in SOFC system. Catal Today 2003;87:255–64. doi:10.1016/J.CATTOD.2003.10.017.
[57] Escudero MJ, Fuerte A. Performance of Ceria-electrolyte Solid Oxide Fuel Cell Using Simulated Biogas Mixtures as Fuel. Adv Energy Power 2017;5:20–6. doi:10.13189/aep.2017.050202.
[58] Barroso Quiroga MM, Castro Luna AE, Kinetic Analysis of Rate Data for Dry Reforming of Methane, Ind. Eng. Chem. Res. 2007; 46:5265-5270

Supplementary materials

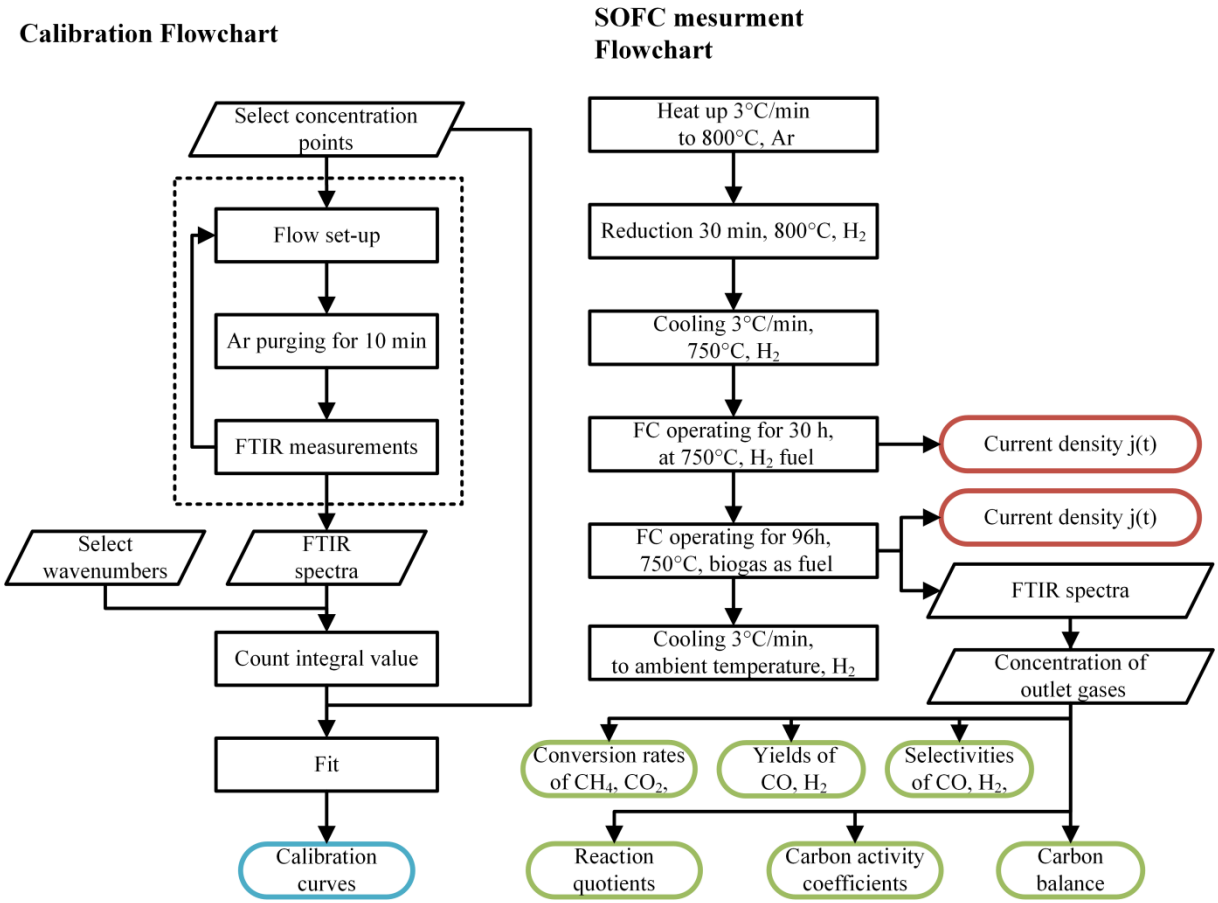

Fig. S1: Schematic view of the measuring procedure for the quantitative analysis of SOFC outlet gases.